Supporting Information

A highly crystalline microporous hybrid organic-inorganic aluminosilicate resembling the AFI-type zeolite

G. Bellussi[1]*, R. Millini[1], E. Montanari[1], A. Carati[1], C. Rizzo[1], W. O'Neil Parker Jr.[1], G. Cruciani[2], A. De Angelis[1] L. Bonoldi[1], S. Zanardi[1]

[1] *eni s.p.a., refining&marketing division, San Donato Milanese Research Center, Via F. Maritano 26, I-20097 San Donato Milanese (Italy).*

[2] *Department of Physics and Earth Sciences, University of Ferrara, Via G. Saragat 1, I-44100 Ferrara (Italy)*

Correspondence to: giuseppe.bellussi@eni.com

Table of Contents

1.   Synthesis of ECS-14

In a typical preparation, 3.05 g (76.2 mmol) of NaOH (Carlo Erba)) and 1.32 g (21.3 mmol) of H_3BO_3 (Fluka, purity > 99%)) were dissolved in 8.83 g of demineralised water at room temperature. 2.02 g of $NaAlO_2$ (54 wt% Al_2O_3, 10.7 mmol of Al_2O_3, Fluka) were then added to the above clear solution and vigorously stirred till a homogeneous gel is formed. Finally, 4.94 g (12.3 mmol) of 1,4-bis-(triethoxysilyl)-benzene (BTEB, JSI Silicone, purity > 98%) were added and the resulting milky reaction mixture was charged into a stainless-steel rotating autoclave. Hydrothermal treatment was performed at 373 K for 4 days under autogeneous pressure. Once cooled to room temperature, the white solid product was separated from the mother liquor by filtration, repeatedly washed with demineralised water and dried overnight at 373 K.

2.   TG-DTA-MS analysis

A Seiko TG/DTA6300 thermobalance, equipped with an alumina furnace capable of reaching 1573 K, was used. This instrument measures simultaneously sample weight loss during heating and the temperature difference between the sample and a reference generating a DTA (Differential Thermal Analysis) curve of the heat absorbed or emitted by the sample. The measurement was made using ca. 10 mg of sample, housed in an alumina crucible placed in the centre of the furnace, with a steady flow of gas equal to 50 ml/min from the bottom of the scale and heating ramps of 5 K/min. An empty crucible was used as a reference. The exit gas from the scale was analysed using an Agilent chromatograph (model. 68501) and an analyzer (mod. 5975) to detect the masses of the flue gas over the 6 to 170 atomic mass unit range. The powdered sample was heated in an oxidizing environment using synthetic air.

TG curve shows three well separated weight losses (Fig. S1a). The first one is accompanied by a slight endothermic event associated to the escape of the water molecules from the ECS-14 porosity as clearly indicated by the masses detected during heating. On the other hand, the second and the third weight losses are accompanied by exothermic peaks (very sharp and intense at 708 K) in the DTA curve. These features are associated to the detection of the masses 18, 44, 76, 77 and 78, indicating that the structural breakdown occurs with both, the combustion of the organic moiety and also the elimination of the integral benzene molecules (Fig. S1b).
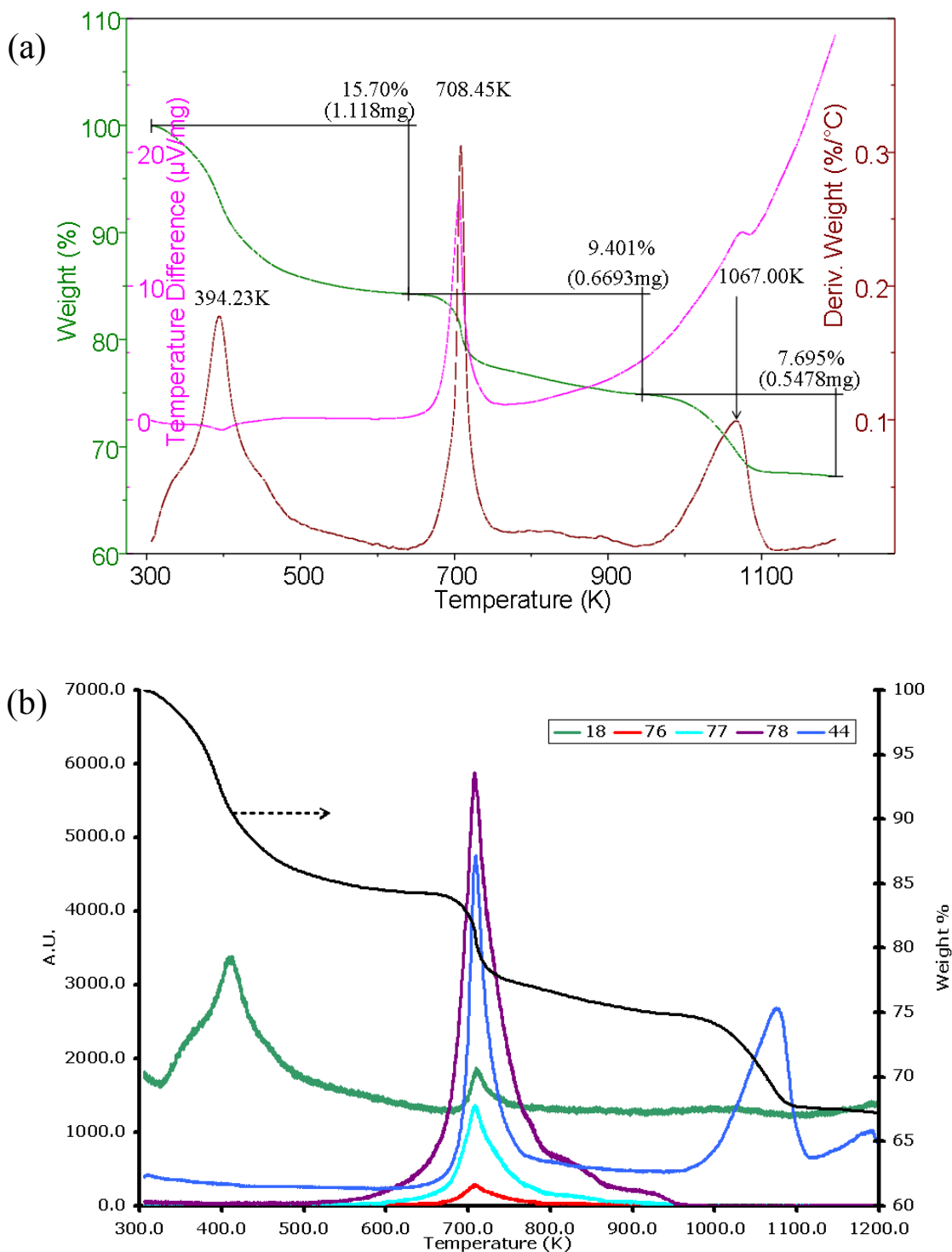
2

(a)

15.70%   708.45K
(1.118mg)

394.23K

9.401%
(0.6693mg)   1067.00K

7.695%
(0.5478mg)

(b)

| 18 | 76 | 77 | 78 | 44 |

Fig. S1. TG-DTA-MS analysis of ECS-14: (a) TG (—), DTG (—) and DTA (—) traces. (b) TG (—) traces and patterns for selected masses detected during the heating ramp.

3

3. ^{29}Si, ^{27}Al, ^{13}C and ^{11}B MAS NMR

Magic Angle Spinning – Nuclear Magnetic Resonance (MAS NMR) spectra were collected with one-pulse Bloch decay (DEPTH for ^{13}C) under conditions of complete relaxation between scans to provide quantitative signal intensities. An Agilent V-500 was used to observe ^{11}B (160 MHz, 0.37 μs = 12° pulse, 2 s delay, shifts referenced to $BF_3 \cdot (OC_2H_5)_3$ at 0 ppm using H_3BO_3 at 19.6 ppm), ^{13}C (126 MHz, DEPTH pulse sequence,[S1] 3.8 μs = 90° pulse, 30 s delay, ^{1}H decoupling, shifts referenced to tetramethylsilane at 0 ppm using adamantane at 38.5 and 29.4 ppm), ^{27}Al (130 MHz, 0.35 μs = 12°, 1 s delay, shifts referenced to aq. $AlCl_3$ at 0 ppm) for samples contained in 4 mm rotors spinning at 14 kHz. A Bruker ASX-300 was used to observe ^{29}Si (59 MHz, 3.8 μs = 60° pulse, 90 s delay, ^{1}H decoupling, shifts referenced to tetramethylsilane at 0 ppm using tetrakis(trimethylsilyl)silane at -9.8 and -135.2 ppm) for samples contained in 7 mm rotors spinning at 5 kHz.

^{29}Si, ^{27}Al and ^{13}C MAS NMR spectra are shown in Fig. S2, ^{11}B MAS NMR spectra of ECS-14 in the as-synthesized form and after treatment with 0.1 M NaOH solution are reported in Fig. S3.
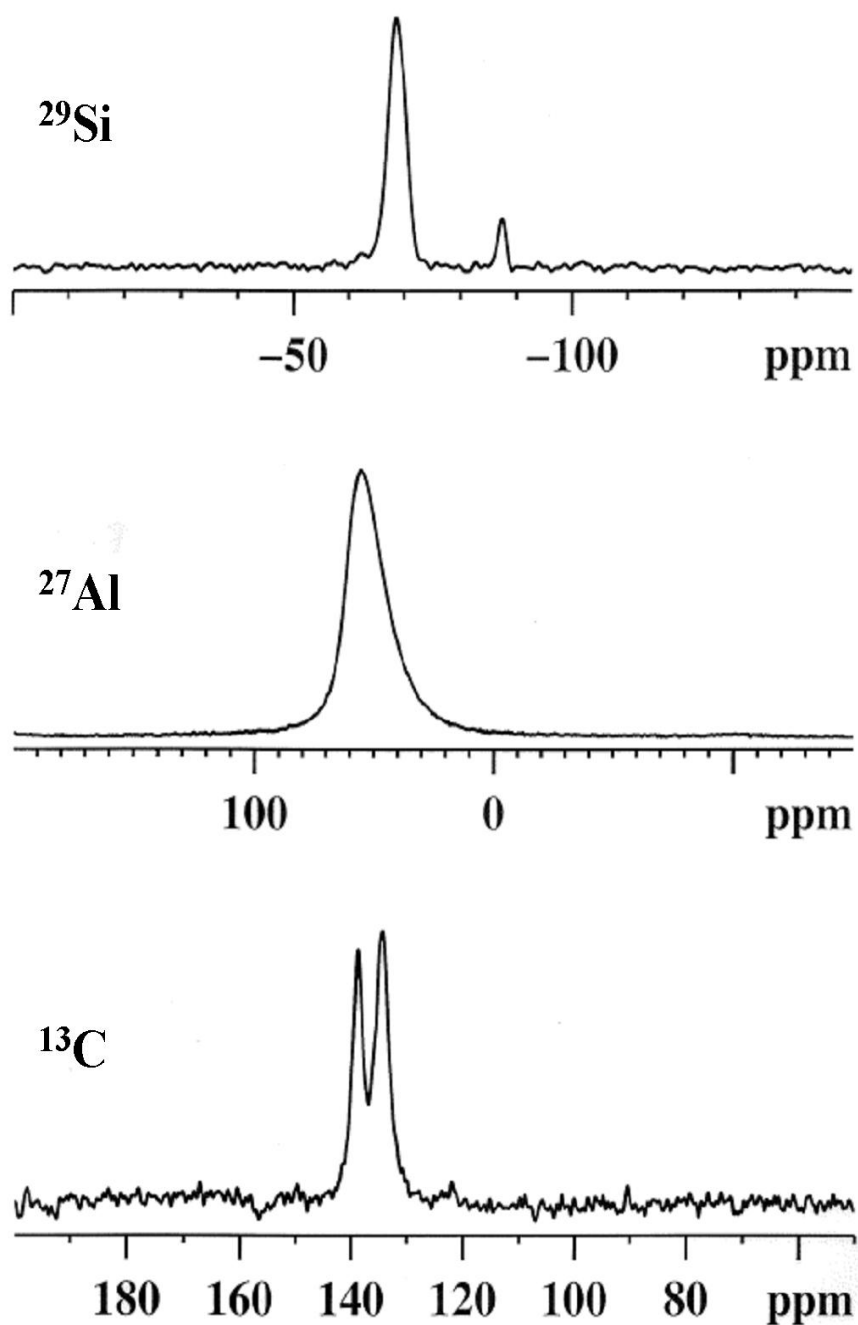
Fig. S2: NMR spectra of ECS-14. a Sharp ^{29}Si MAS NMR signals evidenced two different environments, with silicon mainly bonded to one organic moiety (-68 ppm) and with $Si(OAl)_4$ sites (-87 ppm) from slight carbon-silicon bond cleavage (7%). ^{27}Al MAS NMR spectroscopy reveals tetrahedral coordination for aluminium. The ^{13}C MAS NMR spectrum confirms organic fragment integrity.
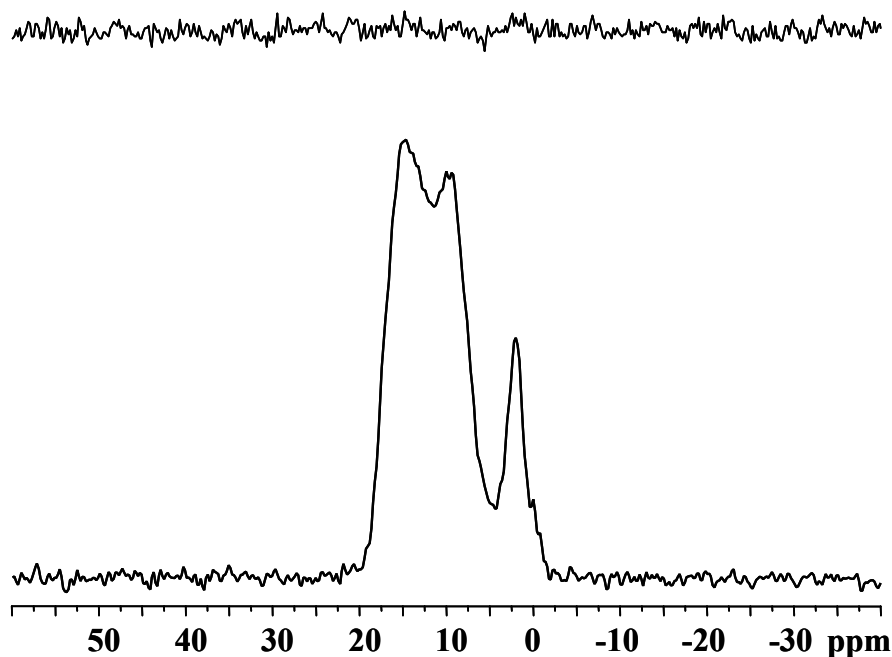
Fig. S3. ^{11}B MAS NMR spectra of ECS-14 before (bottom) and after (top) washing with 0.1 M NaOH solution. Spectra were obtained with an Agilent V-500 (160 MHz, 0.37 μs = 12° pulse, 2 s delay, shifts referenced to $BF_3 \cdot (OC_2H_5)_3$ at 0 ppm using H_3BO_3 at 19.6 ppm) for samples contained in 4 mm rotors spinning at 14 kHz. The ^{11}B MAS NMR spectrum of ECS-14 exhibits mainly a broad pattern (85% of total area) with two singularities, at 15 and 10 ppm, assigned to a BO_3 site, with a smaller sharp signal near 2 ppm assigned to a BO_4 site. After washing, no boron signal was detected.

4. High-resolution synchrotron powder diffraction data collection, structure solution and refinement

The high-resolution synchrotron X-ray powder diffraction data of as-synthesized ECS-14 were collected at room temperature on the ID-31 beamline, at the European Synchrotron Radiation Facility (ESRF, Grenoble (F)), during the experiment CH-3370. The beamline was set to deliver a wavelength of 0.49589(2) Å. The borosilicate glass capillary (1.0 mm i.d.), containing the ECS-14 sample, was spun and translated during data collection to minimize preferred orientation phenomena and radiation damage, respectively. Data were collected in continuous mode over the range $1 \leq 2\theta \leq 50°$ with increasing accumulation times for higher scattering angles and finally rebinned with a step size of 0.001° 2θ.

The high resolution powder pattern has been profile-fitted and fully indexed using the routines contained in different dedicated software (Bruker TOPAS suite, TREOR,[S2] ITO,[S3] DICVOL[S4]) that gave an hexagonal unit cell with parameters $a = b = 14.242$ and $c = 27.206$ Å. The analysis of the systematic extinctions performed using the space group search routine implemented in EXPO2009[S5] gave the highest figure of merit for *P6/mcc*, which was assumed and later confirmed by the structure determination. The ECS-14 crystal structure was achieved *ab-initio* by direct methods as implemented in EXPO2009.[S5] Although re-labelling of some atoms were necessary, a structural model, in which layers are formed by $[CSiO_3]$ and $[AlO_3OH]$ tetrahedra, was readily found. Recycling this structural model in the Fourier routine allowed the allocation of the three crystallographically independent carbons composing the phenylene rings.

The Rietveld refinement, starting from the above obtained structural model was carried out against the HR-XRD with the GSAS software.[S6,S7] Geometric soft constraints were applied to the tetrahedra (Si–O (1.60(5) Å), Al–O (1.71(5) Å), O–O (2.60(1) and 2.80(1) Å depending on the tetrahedrally centred atoms, Si or Al, respectively) and to the aromatic rings (C-C = 1.38(2) and 2.80(2) Å). The constraints weighting factor was gradually decreased during the refinement, yielding reasonable bond lengths. Framework atoms of the same element were constrained to have the same isotropic thermal displacement parameter and subsequently refined.

Significant anisotropic broadening of the reflections were observed in the synchrotron X-ray powder diffraction pattern, this phenomenon was accounted for by including different terms in the pseudo-Voigt peak shape function during the refinements (parameters 'stec' and 'ptec' in the GSAS function n° 2). Anisotropic broadening can be clearly appreciated from Fig. S4, where

sharp 100, 110 and 211 reflections are close to broad $00l$ (l = 2, 4 and 6) reflections. This phenomenon can be mainly attributed to the ECS-14 morphology that crystallizes in plate-like hexagonal shapes, well evidenced by the SEM micrographs in Fig. 1. However, some stacking fault can not be ruled out considering the relatively good (but not excellent) discrepancy RF^2 factor (Tab. S1).
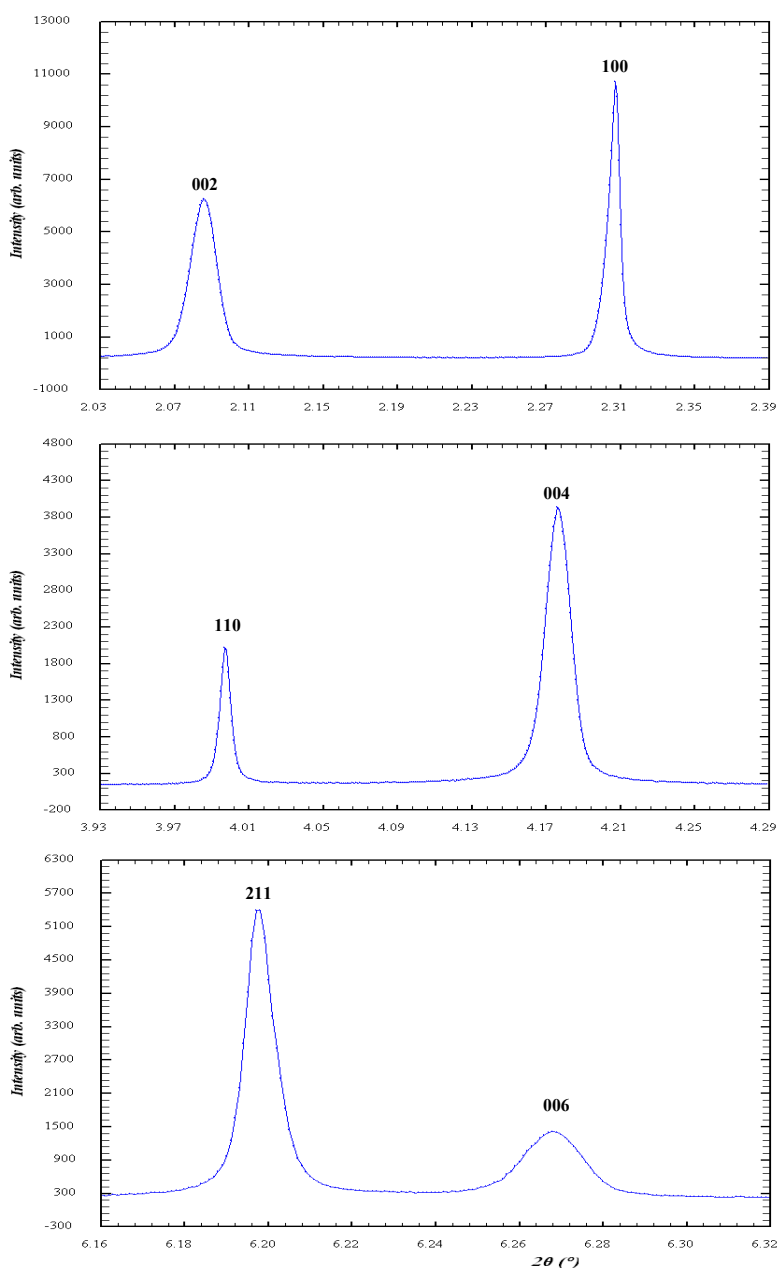

Fig. S4: Portions of the high-resolution SXPD pattern of ECS-14. The anisotropic line broadening associated with the ECS-14 crystallite morphology, and affecting the 00l reflection, is shown.

Tab. S1: Structural and refinement parameters for ECS-14

Crystal system	Hexagonal
Space Group	P6/mcc
a (Å)	14.21306(3)
c (Å)	27.2081(1)
V (Å^3)	4759.97(3)
RF^2 (%)	14.1
Rp (%)	4.6
Rwp (%)	6.4
χ^2	9.02
No. observations	38525
No. reflections	2329
No. parameters	123
No. of geometric restrains	26
2θ range used in the refinement (°)	1.5-40

The final Rietveld refinement converged to a satisfactory reproduction of the experimental profile, in spite of the difficult modelling of the anisotropic peak broadening due to the ECS-14 crystallite shape (Fig. S5).

Careful inspection of the Fourier maps allowed discrimination of nine extra-framework positions. Among them, three were attributed to sodium cations on the basis of occupancy factor and the bond distances from the framework oxygens or water molecules. Aware of the correlation between occupancy parameters and the temperature factors, the two parameters have been refined separately and not simultaneously. At the final refined cycle, the extra-framework occupancies corresponded to 648 electrons in fairly good agreement with those calculated by TG + chemical analyses (634). The obtained displacement factors are in line with those reported for some single crystal studies carried out on large pore zeolites with strong disorder of extra-framework cations and water molecules in the channels (i.e. the natural zeolites tschernichite,[S8-S9] boggsite,[S10] gottardiite,[S11] natural and synthetic mordenite[S12]).
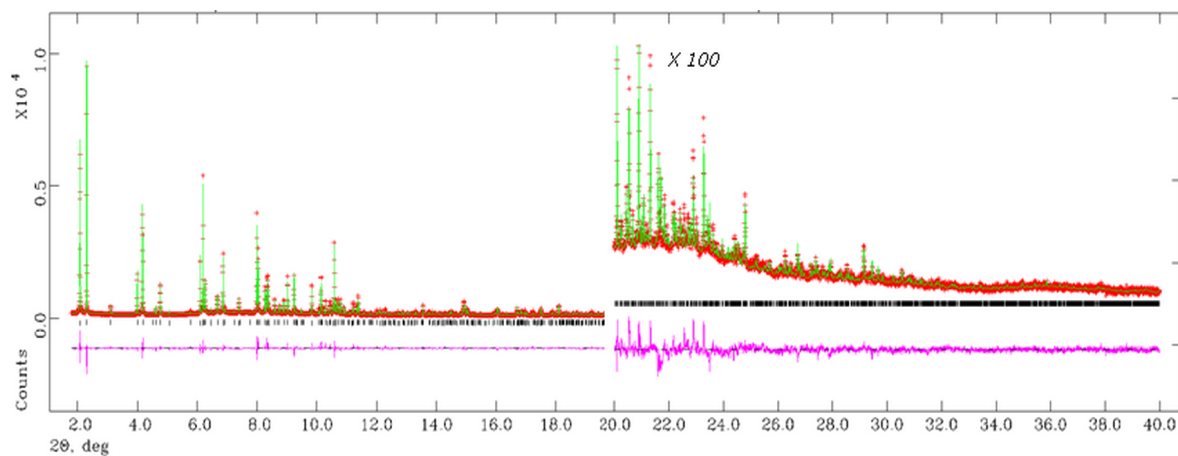
9

Fig. S5: Observed (+), calculated (—), and difference (—) profiles for Rietveld refinement. The higher angle data are vertically expanded by a factor of one hundred to show more details.

Selected bond distances are listed in Tab. S2.

Tab. S2: Selected bond distances for ECS-14

Si1 – O1	1.650(3)	Na1 – O1	3.080(4)
Si1 – O2	1.606(4)	Na1 – O1	3.081(3)
Si – O3	1.583(4)	Na1 – O1	3.081(3)
Si – C1	1.899(3)	Na1 – O3	2.376(3)
		Na1 – O3	2.376(3)
Al1 – O1	1.633(4)	Na1 – O3	2.377(4)
Al1 – O2	1.733(3)		
Al1 – O3	1.775(4)	Na2 – O1 × 4	1.926(3)
Al1 – O4	1.705(3)		
Mean	1.712(2)	Na3 – W5 × 6	2.675(9)

5.   Other physico-chemical characterization techniques

Morphological characterization was performed by Field Emission Scanning Electron Microscopy (FESEM) using a JEOL 7600F high-resolution microscope with field emission source for hot cathode Schottky type, secondary electron detector "semi-in-lens"; the acceleration of the electron varying from 0.1 to 30 kV and a maximum resolution is of 1.0 nm at 15 kV. Samples were dispersed in isopropanol, subjected to ultra-sonication and evaporated on the stab for analysis.

The as-synthesized sample was analyzed for SiO_2 by gravimetry after calcination at 1173 K in air, Al, B and Na by Induced Coupled Plasma-Optical Emission Spectroscopy (ICP-OES) using a Thermo Optec ICAP6500 dual view analyzer. CHN analyses were carried out by ELEMENTAR MACRO CHNS analyzer.

Density measurement was carried out on the as-synthesized ECS-14 sample by using a Micromeritics Accupyc 1330 He displacement pycnometer.
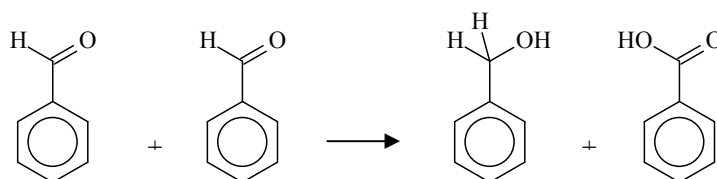
6.   Catalytic tests

The high Na^+ content makes ECS-14 an ideal candidate for basic catalysis. Its catalytic properties were therefore compared to those of Zn-Al and Mg-Al hydrotalcites, which are very active basic catalysts, in the Claise-Schmidt condensation of benzaldehyde and acetophenone to (2E)-1,3-diphenyl-2-propen-1-one (trans-Chalcone) chosen as a test reaction (Scheme S1).

A mixture of benzaldehyde (17.76 mmol), acetophenone (14.8 mmol) and the solid catalyst (ECS-14, hydrotalcite $[Zn_6Al_2(OH)_{16}]CO_3$ or $[Mg_4Al_2(OH)_6](NO_3)_2$, 5 wt.% referred to acetophenone) was added to a three-neck flask and heated under reflux, under vigorous stirring. The reaction was monitored by ^{13}C NMR spectroscopy of aliquots taken at different reaction times. Tests were performed to verify the presence of basic sites in ECS-14 and to evaluate their strength relative to other non-porous basic catalysts.
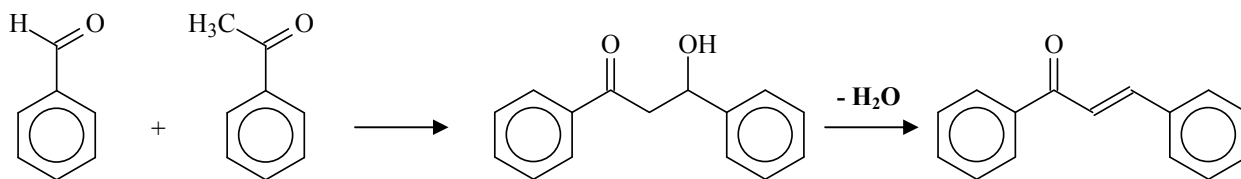
Scheme S1

This reaction requires a basic catalyst with medium strength. High basicity causes the disproportionation of benzaldehyde to benzyl alcohol and benzoic acid (Cannizzaro's reaction) (Scheme S2).

Scheme 2S

The results of the catalytic tests are reported in Tab. S3.

Table S3. Results of the catalytic tests compared with those reported in ref. S13.

Catalyst	Reaction time (hours)	Acetophenone conversion (%)	trans-chalcone selectivity (%)	cis-chalcone selectivity (%)
ECS-14	3	46.7	100	0
	6	87.0	100	0
Zn-Al	3	8.7	100	0
	6	10.9	100	0
Mg-Al	3	17.4	100	0
	6	23.9	100	0
NaOH[*]	2	not given	89	3

* benzoic acid and benzyl alcohol were produced with 2% selectivity each

13

7. Optical properties

Thanks to the presence of organic units, ECS-14 shows also very interesting optical properties. In spite of the high concentration, the phenylene units are still emissive, similarly to what happens in ECS-2 and is reported for other hybrid materials.[S14] In Fig. S6a the fluorescence spectrum of both materials is reported together with that of the BTEB precursor in cyclohexane solution. ECS-14 emits at almost the same wavelength as the precursor, at variance with ECS-2, whose emission band is red-shifted signalling an electronic interaction that does not occur in ECS-14 in agreement with the different configuration of aromatic rings. In ECS-14 they are disposed in sequence along the channel section, while in ECS-2 they are present as couples of stacked units at 3.4 Å distance (see Fig. S4b). The concurrent presence of open porosity with straight channel and high density of emissive species makes ECS-14 particularly suitable for application in antenna systems,[S15] as the supporting host and the donor at the same time.[S16] In addition, the perfectly ordered arrangement of aromatic units in channel walls can be exploited to optimize the energy transfer to the emissive guest. The porosity and the optical properties could also find application also in sensing devices.
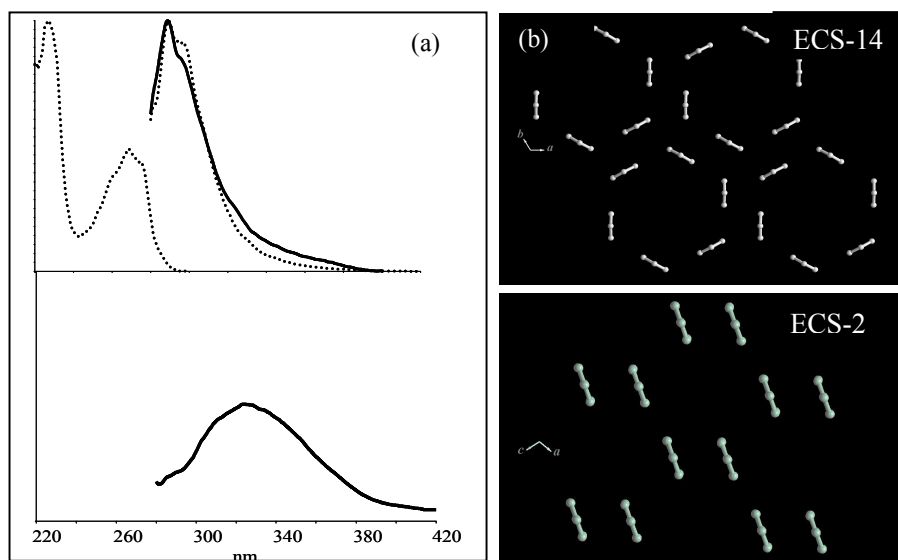

Fig. S6: (a) Schematic representation of the aromatic rings arrangement in ECS-14 and ECS-2. (b) Emission spectra of ECS-14, ECS-2 (continuous trace; λ_{exc} = 270 nm) with the excitation and emission spectra of the precursor BTEB in diluted cyclohexane solution (dotted trace).

14

Fluorescence spectra were collected at room temperature with a Perkin Elmer LS50 Spectrofluorometer with 3.5 nm bandwidth and were corrected for the spectral response of the system. The precursor was analysed in dilute cyclohexane solution; the solids were mixed and grounded with KBr at 5 % weight/weight and measured in front face configuration with 30°/60° geometry and a 10 % neutral filter in emission to reduce the strong fluorescence intensity.

References

S1. DEPTH has a composite (90°-180°-180°) excitation pulse with 16-phase cycling (onepuldpth.c) to suppress the signal from the Kel-F spacers, adapted from M. R. Bendall and R. E. Gordon, *Magn. Reson. Med.*, 1985, **2**, 91

S2. P. E. Werner, L. Eriksson, M. Westdahl, *J. Appl. Crystallogr.*, 1985, **18**, 367

S3. J. W. Visser, *J. Appl. Crystallogr.*, 1969, **2**, 89

S4. A. Boultif and D. J. Löuer, *J. Appl. Crystallogr.*, 1991, **24**, 987

S5. A. Altomare, M. Camalli, C. Cuocci, C. Giacovazzo, A. Moliterni and R. Rizzi, *J. Appl. Crystallogr.*, 2009, **42**, 1197

S6. A. C. Larson and R. B. Von Dreele. Los Alamos, National Laboratory Report LAUR-86-748, 2000.

S7. B. H. Toby. *J. Appl. Crystallogr.*, 2001, **34**, 210

S8. Alberti et al., *J. Phys. Chem. B* 2002, **106**, 10277-10284

S9. Alberti et al., *J. Phys. Chem. C* 2007, **111**, 4503-4511

S10. Zanardi et al., *Amer. Mineral.*, 2004, **89**, 1033–1042

S11. Alberti et al., *Eur. J. Miner.* 1996, **8**, 69-75

S12. Simonic and Ambruster, *Amer. Mineral.*, 2004, **89**, 421–431

S13. M. J. Climent, H. Garcia, J. Primo and A. Corma, *Catal. Lett.*, 1990, **4**, 85

S14. N. Mizoshita, H. Tani and S. Inagaki, *Chem. Soc. Rev.*, 2011, **40**, 789

S15. G. Calzaferri, S. Huber, H. Maas and C. Minkowski, *Angew. Chem. Int. Ed.*, 2003, **42**, 3732

S16. S. Inagaki, O. Ohtani, Y. Goto, K. Okamoto, M. Ikai, K. Yamanaka, T. Tani and T. Okada, *Angew. Chem. Int. Ed.*, 2009, **48**, 4042